

Investigation on Double-Pass Configurations for Thomson Scattering Measurements

Yi PENG, Akira EJIRI, Yuichi TAKASE, Naoto TSUJII, Osamu WATANABE, Kotaro IWASAKI, Yongtae KO, James Hamilton Palmer RICE, Yuki OSAWA, Go YATOMI, Iwao YAMADA, Takeshi IDO¹⁾, Yoshihiko NAGASHIMA¹⁾ and Kaori KONO¹⁾

The University of Tokyo, Kashiwa 277-8561, Japan

¹⁾*Kyushu University, Kasuga 816-8580, Japan*

(Received 31 August 2020 / Accepted 13 January 2021)

Double-pass Thomson scattering is a simple and reliable scheme to measure two-directional (perpendicular and parallel) electron temperatures in plasmas. In this study, we configured a double-pass Thomson scattering configuration so that the laser beam passing through plasma is reflected by a mirror and passes through the plasma again to generate the second scattering light with a different scattering angle. To avoid direct re-entering of the beam to the laser, the reflected beam was tilted slightly. This study investigated the configuration in terms of the measurement performance and laser damage risk by the backward beam. Furthermore, this study clarified several requirements on the optical configuration and quantified the parameters' effects on the performance of the configuration. Through optimization procedures, three optimal configurations were figured out: (i) a simple configuration with two lenses and one mirror, but with a long distance from the laser to the plasma, (ii) another simple configuration that slightly breaks the requirement of sufficient deviation of the backward beam from the laser output, and (iii) a modified configuration with three lenses and one mirror.

© 2021 The Japan Society of Plasma Science and Nuclear Fusion Research

Keywords: Thomson scattering, double-pass, Gaussian beam, requirement of double-pass configuration, optimal double-pass configuration

DOI: 10.1585/pfr.16.1402027

1. Introduction

The Thomson scattering diagnostic is a reliable and non-intrusive way of measuring electron temperature and density in plasma. The isotropic Maxwellian velocity distribution function describes the plasmas in the thermal equilibrium. However, almost all heating methods heat particles anisotropically and may invoke anisotropic temperature. By measuring the forward and backward scattering lights, we can measure the distribution functions along the two directions (perpendicular and parallel to the magnetic field) when the Thomson scattering angle (i.e., the angle between the laser beam and the collection optics' optical axis) is far from 90°. The electron temperature anisotropy was found in ECH (electron cyclotron heating) plasmas using Thomson scattering scheme [1, 2]. For inductive electric field heating (i.e., standard Ohmic heating), different temperatures in the parallel, the perpendicular, and the anti-parallel directions with respect to magnetic field direction were found by a double-pass Thomson scattering scheme [3], and the experimental results were compared with theoretical expectation [4]. Temperature anisotropy measurement helps understanding the heating and current drive mechanisms and temperature anisotropy-driven instabilities [5].

The double-pass Thomson scattering scheme [6],

author's e-mail: peng-yi@g.ecc.u-tokyo.ac.jp

where a mirror is used to reflect the incident beam back into the plasma, is the simplest scheme to measure the forward and backward scattering signal with a single collection optics. However, the backward beam should be tilted slightly to avoid its re-entering to the laser. The tilt should be large enough to avoid the risk of the re-entering and resultant laser damage, but the risk is not a simple function of the tilt degree, as shown in Sec. 6. Therefore, there is a need for more reliable and quantitative assessment of the risk. The tilt degree should be small to minimize the difference between the forward and backward optical passes in the plasma. Thus, configuration optimization is an important issue for the double-pass configuration. A coaxial multipass Thomson scattering scheme is used to trap the laser beam in a cavity by a Pockels cell using an optical switch [7, 8]. The optics' major part is simple, but its fine adjustment and electrical setup in achieving a good trap are not easy, especially when the laser is unstable at the beginning of laser operation, because the forward and backward beams need to be aligned. Although the double-pass scheme is robust and simple, theoretical analyses of the measurement performance and the risk are still required for configuration optimization. An optical isolator can block the backward laser beam; however, we experienced laser damage even with an isolator. Hence, there is a need to understand the situation quantitatively.

The rest of this paper is organized as follows. Section 2 describes the double-pass configuration. Section 3 gives the simulation model. Section 4 discusses several requirements indicating the configuration's performance. Section 5 shows the free parameters' effects on the requirements. Section 6 discusses the optimization procedure in acquiring optimal configurations, and Sec. 7 concludes this study.

2. Optical Configuration

Figure 1 shows the basic and minimum double-pass configuration and the variables' definitions used in this study. The laser beam passes through the plasma, and then the first measurement is carried out in a standard single-pass configuration. The laser beam is reflected by a mirror and re-enters the plasma, and then the second measurement is performed. The mirror should be located far (e.g., several meters) from the plasma to distinguish the scattering signals by a fast-response detector (such as shown by Ejiri *et al.* [9]). The system should contain optical components to enable the long distance propagation of laser beam. The configuration consists of (i) a laser source (with a beam quality factor M , wavelength λ , and beam waist w_0), (ii) two convex lenses (focal length: f_1 and f_2 ; diameter: D_{f1} and D_{f2} ; and the beam arriving at f_1 and f_2 has the beam radii of w_{f1} and w_{f2}), (iii) an endmost mirror that is tilted slightly (tilting angle should be $\delta\theta/2$ to reflect the beam at an angle of $\delta\theta$) and makes the reflected beam (orange color) deviate from the original beam (red color), (iv) collection optics consisting of a collection lens (focal length: f_{col} ; radius: R_{col}), and (v) a fiber with the radius R_{fiber} . s_1 and s_2 indicate the distance between the focus and the lens and between the lens and the fiber, respectively. A concave mirror with the focal length of $f_2/2$ can replace the second lens and the endmost mirror placed at the end of the configuration. (the difference has not been discussed owing to its irrelevance in this work.) Similarly, a concave mirror can replace the collection lens. The scattering angle which is not discussed in this study, affects the temperature anisotropy measurements' performance [4]. In Fig. 1, we assumed that the scattering angle is 90° and the focal point (with the beam radius w_p) of the two lenses is located at the plasma center. We neglected the vacuum windows or apertures that may limit the beam size or cut beam's part. There is a displacement of the backward beam at the plasma center (δ_p), lens f_1 (δ_{f1}), and laser outlet (δ_{laser}) because of the tilted mirror. We assumed that a Gaussian beam represents the beam and that the beam's waist size w and waist position (i.e., focal point) are calculated from the modified formulas for Gaussian beams, including M^2 . Moreover, the deviation of backward beam axis from the forward optical axis is calculated from geometrical optics. The following describes the laser beam propagation process. The laser beam emitted from the laser source passes through the first lens and is focused at the plasma's center. A collection lens

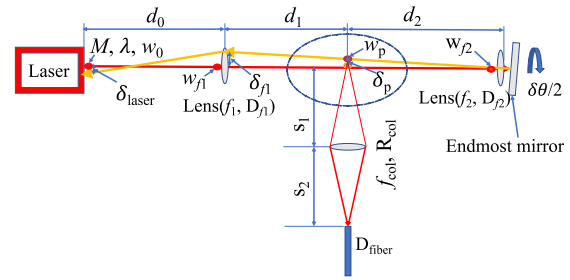


Fig. 1 Schematic configuration of the double-pass scheme.

collects the scattered light, which is focused on a fiber surface. After that, the laser beam passes through the plasma and hits the second lens as well as the endmost mirror. The second lens enables the reflected beam to have a focal point at the plasma center (the same point as in the first pass). The endmost mirror can be tilted, so that the second pass is deviated from the first pass. This is important for the reflected beam as it helps not to hit the laser. Hereafter, we denoted the beams in the first and second passes as the forward and backward beams, respectively. We can block the power without cutting the forward beam if the deviation (i.e., shift) is sufficiently large. For example, we may place a beam dump near the first lens or the laser output. It is easy to block the backward beam when the shift is large, but the measurement points inside the plasma may also shift significantly from that of the forward beam, leading to a temperature variation because of the temperature profile. This temperature variation becomes a systematic error for the temperature anisotropy measurement; hence, it should be minimized. In addition, the shift may deteriorate the scattered light's collection efficiency.

3. Simulation Model

In many laser applications, the laser beam can be considered as a Gaussian beam, in which the intensity distribution is written as follows [10]:

$$I(r, z) = I_0 \exp(-2r^2/w(z)^2) = 2P/\pi w(z)^2 \exp(-2r^2/w(z)^2), \quad (1)$$

where I_0 is the peak intensity at the beam profile's center, r denotes the radial distance away from the beam axis, $w(z)$ indicates the beam radius where the intensity becomes $1/e^2$ of I_0 , z is the coordinate along the propagation direction, and P is the beam's total power. In addition, the beam radius $w(z)$ is

$$w(z) = w_0 \sqrt{1 + (z/z_R)^2}, \quad (2)$$

$$z_R \equiv (\pi w_0^2/\lambda M^2), \quad (3)$$

where w_0 is the radius of the beam waist ($z = 0$), z_R is the Rayleigh range, and M is the beam quality factor. Suppose the waist radius (w_0) and the distance (d_0) between an object and a thin lens (with focal length f) are given. In that

case, the following formulas can be used to calculate the image distance d_i away from the lens and the image radius w_i (i.e., the radius of the beam waist):

$$d_i = \frac{\left(\left(\frac{\pi w_o^2}{\lambda M^2}\right)^2 \frac{1}{f} - d_o \left(1 - \frac{d_o}{f}\right)\right)}{\left(\left(\frac{\pi w_o^2}{\lambda M^2}\right)^2 \left(\frac{1}{f}\right)^2 + \left(1 - \frac{d_o}{f}\right)^2\right)}, \quad (4)$$

$$w_i = w_o / \sqrt{\left(\frac{\pi w_o^2}{\lambda M^2}\right)^2 \left(\frac{1}{f}\right)^2 + \left(1 - \frac{d_o}{f}\right)^2}. \quad (5)$$

These formulas are used in the design and calculations for the double-pass configuration.

The simulation is working on the assumption that the beam sizes are calculated assuming Gaussian beams, and that the axis of the backward beam is calculated on the basis of paraxial and thin lens approximations. The following describes the simulation process. For the forward beam, the expression of the focal length f_1 could be deduced from Eq. (4) if the distances d_0 and d_1 are preset.

$$f_1 = \frac{(z_{R0}^2 + d_0^2 + 2d_0d_1) - \sqrt{(z_{R0}^2 + d_0^2)^2 - 4d_1^2 z_{R0}^2}}{2(d_0 + d_1)}. \quad (6)$$

The beam radius calculation at the first lens (w_{f1}) is calculated from Eq. (2): $w_{f1} = w_o \sqrt{1 + (d_0/z_{R0})^2}$. After the laser beam goes through the first lens, the beam radius at the plasma center (w_p) is obtained from Eq. (5).

$$w_p = w_o / \sqrt{\left(\frac{\pi w_o^2}{\lambda M^2}\right)^2 \left(\frac{1}{f_1}\right)^2 + \left(1 - \frac{d_0}{f_1}\right)^2}. \quad (7)$$

Similarly, the beam radius at the second lens w_{f2} is calculated as $w_{f2} = w_p \sqrt{1 + (d_2/z_{Rp})^2}$. After the forward beam hits the endmost mirror, it turns into the backward beam, and f_2 needs to be determined similarly for the given d_2 to focalize the laser beam at the plasma center.

$$f_2 = \frac{3d_2^2 + z_{Rp}^2 - \sqrt{(d_2^2 - z_{Rp}^2)^2}}{4d_2}. \quad (8)$$

However, there is a displacement (δ_p) of the backward beam (compared with the focus of the forward beam) at the plasma center because of the tilting mirror. It is reasonable to consider δ_p as a free independent parameter because we can rotate the endmost mirror manually. Besides, the displacement will affect the efficiency of the collection optics, and a variable would be introduced here, the relative intensity E_c , which indicates the relative collection efficiency of the backward scattering signal compared with the forward scattering signal.

Figure 2 shows the schematic drawing of the collection optics and the shift's effect of the backward beam (orange spot) from the forward beam (red spot); the beam axes are perpendicular to the figure. The collection optics

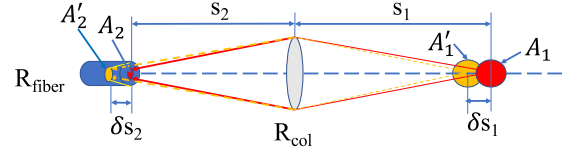


Fig. 2 Schematic diagram of the collection optics.

is designed for the scattering light from the forward beam to be focused at the center of the fiber. When the backward beam is shifted by δs_1 , the focus point is shifted by δs_2 from the fiber surface. When $\delta s_1 \ll s_1$, δs_2 is proportional to δs_1 , and δs_2 causes defocusing, resulting in decreased efficiency of the scattering light collection. We evaluated the effect on the following. A_1' represents the scattering area of the backward beam seen from the collection optics (i.e., the beam's area perpendicular to the collection optics' axis). A_2' indicates the corresponding area at the focus point near the fiber. A_1 and A_2 are the corresponding forward beam's scattering areas. In Fig. 2, the conservation of etendue (i.e., the product of the solid angle and area) is written as follows:

$$\begin{aligned} L_1 &= 2 \cdot R_{fiber} \cdot s_1 / s_2, \\ L_1' &= 2 \cdot R_{fiber} \cdot (s_1 - \delta s_1) / (s_2 + \delta s_2), \\ \Omega_1 A_1' &= \Omega_2' A_2', \quad \Omega_1 A_1 = \Omega_2 A_2, \end{aligned} \quad (9)$$

where L_1 and L_1' are the scattering lengths of the forward and backward beams, respectively; Ω_1' is the solid angle that the area of the collection lens subtends to the scattering point of the backward beam; and Ω_2' is the solid angle formed at the collection side. Similarly, Ω_1 and Ω_2 are the solid angles formed by the corresponding forward scattering. We also assumed that the fiber collects all the forward beam's scattering signals if we arranged the appropriate s_1 and s_2 . The following equations give the expressions of Ω_1' and Ω_2' in Fig. 2:

$$\Omega_1' = \pi R_{col}^2 / (s_1 - \delta s_1)^2, \quad (10)$$

$$\Omega_2' = \pi R_{col}^2 / (s_2 + \delta s_2)^2. \quad (11)$$

There is an additional important solid angle that is subtended by the area of the fiber inlet (Ω_3'), and it represents an effective amount of the collected signal entering the fiber. Its expression is given by the following Eq. (12).

$$\Omega_3' = \pi R_{fiber}^2 / (\delta s_2)^2. \quad (12)$$

When δs_2 is very small, Ω_3' becomes large (e.g., > 1) and the approximate expression is not valid; however, in such a case, the effect of defocusing is negligible. Combining Eqs. (9) - (12), we could formulate the relative collection efficiency as follows:

$$\begin{aligned} E_c &= \frac{\Omega_3' A_2'}{\Omega_1 A_1} = \frac{\Omega_3'}{\Omega_1 A_1} \cdot \frac{\Omega_1' A_1'}{\Omega_2'} \\ &= \frac{s_1 \cdot s_2 \cdot (s_2 + \delta s_2)}{(s_1 - \delta s_1) \cdot (\delta s_2)^2} \cdot \left(\frac{R_{fiber}}{R_{col}}\right)^2, \end{aligned} \quad (13)$$

and it should be > 1 to keep all the scattering signals going into the fiber. Furthermore, we estimated the effects of the scattering-beam spot height on the collection efficiency for the backward beam with $\delta_{s1} \neq 0$, and the result shows a very small collection efficiency deterioration ($< 1\%$) for a typical case; such an effect is neglected in this study.

After the backward beam passes the plasma region again, it is directed to the first lens (f_1) with a deviation from the forward beam's optical axis. The deviation could be estimated on the basis of geometric optics and paraxial approximation. Therefore, we can express the deviation δ_{f1} as $\delta_{f1} = \delta_p(d_1 + d_2)/d_2$, which is dependent on the free variables d_1 , d_2 , and δ_p . Thereafter, the first lens refracts the backward beam as it is going through f_1 , and then the backward beam finally reaches the vicinity of the YAG laser device's output. The backward beam's displacement could be given by the expression $\delta_{laser} = \frac{\delta_p}{d_2} \cdot \left| d_0 \cdot \left| 1 - \frac{d_1 + d_2}{f_1} \right| - d_1 - d_2 \right|$, and it is related to all the free parameters d_0 , d_1 , d_2 , and δ_p . It is necessary to investigate the dependent variables by scanning the free independent parameters to find feasible double-pass configurations.

4. Requirement List

A double-pass configuration enables the measurements of electron temperature anisotropy; thus, it has to satisfy several requirements to ensure accurate measurement performance (i.e., signal intensity and temperature accuracy) and reduce the laser damage risk caused by the backward beam. The following shows the requirements and their derivations.

The beam radius should be much smaller than the optical components' size; otherwise, the beam is distorted by diffraction, and we cannot assume a Gaussian beam propagation. We should consider the beam radii at the first lens (w_{f1}), the second lens (w_{f2}), and the fiber surface (mw_p). Here, $m = s_2/s_1$ is the magnification of the collection optics. On the basis of the Gaussian profile, we adopted a factor of 4 for the minimum ratio of the diameter of an optical component to the beam radius w , presented as follows. Note that the power outside this diameter is 0.06% of the total power.

$$4w_{f1}/D_{f1} \leq 1, \quad (14)$$

$$4w_{f2}/D_{f2} \leq 1, \quad (15)$$

$$4mw_p/D_{\text{fiber}} \leq 1, \quad (16)$$

where D_{f1} , D_{f2} , and $D_{\text{fiber}} (= 2R_{\text{fiber}})$ denote the diameters of the first lens, second lens, and fiber, respectively.

The shift of the backward laser beam causes a systematic temperature error ΔT . Assuming that the temperature scale length is a (which is the minor radius' order), the temperature difference due to the spatial displacement δ_p of the backward beam is $\Delta T/T \sim \delta_p/a$. If a maximal temperature error of $\alpha_{\text{max}} = \Delta T_{\text{max}}/T$ is required from this

effect, then the requirement is written as follows:

$$\delta_p/(a \cdot \alpha_{\text{max}}) \leq 1. \quad (17)$$

The spatial deviation δ_p may also deteriorate the scattering light collection efficiency. Suppose that the collection optics are adjusted to focus the scattering light from the forward beam on the fiber surface center; then the scattered signals' intensity falling on the fiber surface would decrease if the displacement δ_p (along the collection optics' optical axis) is long. If we assume that the intensity for the case $\delta_p = 0$ is limited by the size of the collection lens; then, the relative intensity (i.e., efficiency) E_c for the case $\delta_p \neq 0$ can be written as a function of the displacement (δ_p), the radius of the fibers (R_{fiber}), the radius of the collection lens (R_{col}), and the spot size at the plasma center (w_p),

$$E_c = \frac{s_1 \cdot s_2 \cdot (s_2 + \delta s_2)}{(s_1 - \delta_p) \cdot (\delta s_2)^2} \cdot \left(\frac{R_{\text{fiber}}}{R_{\text{col}}} \right)^2 \geq 1, \quad (18)$$

where $\delta s_2 = (f_{\text{col}}(s_1 + s_2 - \delta_p - 2w_p) - s_1 s_2 + s_2(\delta_p + 2w_p))/(s_1 - f_{\text{col}} - \delta_p - 2w_p)$ and $f_{\text{col}} = s_1 s_2/(s_1 + s_2)$.

We required that the calculated efficiency $E_c \geq 1$; note that this is physically incorrect, but is useful in showing the margin.

The pulses should be separated in the time domain to split the two (forward and backward) scattering signals by a single detector. In practice, the detector and its circuit determine the signal pulse width Δt_{pulse} . Here, the pulse width is defined as the duration between the beginning of rise and the ending of fall for the signal. For TST-2, Δt_{pulse} is approximately 40 ns [11]. The delay time between the forward and backward scattered signals is denoted by Δt_{delay} . The condition for splitting the pulses is given by

$$\Delta t_{\text{pulse}}/\Delta t_{\text{delay}} \leq 1, \quad (19)$$

where Δt_{delay} is calculated by $2d_2/c$, where c is the speed of light.

The tilted backward beam would be refracted by the first lens and reach a point near the laser, as shown in Fig. 1. We may put an aperture or a beam dump at the points: near the first lens or near the laser output. Therefore, at least one of the displacements of the backward beam at these positions δ_{f1} and δ_{laser} should be significantly larger than the beam size at each point. Then, we can block the backward beam and avoid the laser damage risk. Thus, we set the requirement as follows. A factor of 4 is adopted (Fig. 3), and the unblocked power inside the diameter of $4w$ for the forward beam is less than 0.03%.

$$\text{Min} \{4w_{f1}/\delta_{f1}, 4w_0/\delta_{\text{laser}}\} \leq 1, \quad (20)$$

where $\delta_{f1} = \delta_p(1 + d_1/d_2)$ and $\delta_{\text{laser}} = \delta_{f1}(1 + d_0/(d_1 + d_2) - d_0/d_1)$.

We assumed that the forward and backward beams have a focus at the plasma center, and their propagation

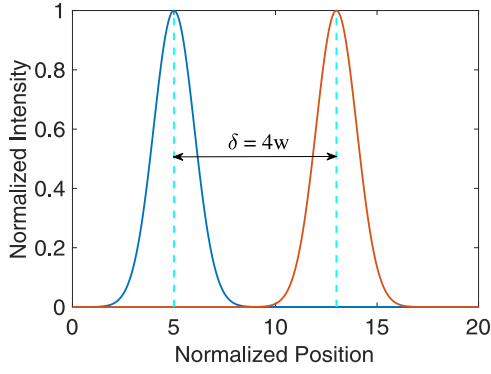


Fig. 3 Two Gaussian profiles with the separation distance of $\delta = 4w$.

is symmetric against the endmost mirror. We can find f_2 for any d_2 , but d_1 and d_2 should have a focus at the plasma (i.e., we should arrange the lenses properly; otherwise, the beam diverges rather than converges after the lens). The condition is written as

$$(2z_{r0}d_1 - z_{r0}^2)/d_0^2 \leq 1, \quad (21)$$

$$(d_2^2 - z_{rp}^2)^2 \geq 0, \quad (22)$$

where $z_{r0} = \pi w_0^2/\lambda M^2$ and $z_{rp} = \pi w_p^2/\lambda M^2$ are the Rayleigh ranges for the laser source and the focus in the plasma, respectively.

It is reasonable to classify the variables into three kinds: fixed, free independent, and dependent parameters. We can choose the free independent parameters by determining the optical configuration and measurement accuracy. Therefore, we have to find (optimize) the best set of the free independent parameters in terms of safety and accuracy, as the requirements listed in Sec. 4. The fixed parameters include the YAG laser's specification and the optical components' size. The free independent parameters can be chosen, and the dependent parameters could be obtained from other parameters. The following shows the list of parameters and classifications.

- Fixed parameters: w_0 , λ , M , s_1 , s_2 , α , α_{\max} , D_{f1} , D_{f2} , R_{col} , R_{fiber} , and Δt_{pulse} .
- Free independent parameters: d_0 , d_1 , d_2 , and $\alpha = \delta_p/a$.
- Dependent parameters: f_1 , f_2 , w_{f1} , w_p , w_{f2} , f_{col} , E_c , Δt_{delay} , δ_{f1} , and δ_{laser} .

The effects of each free independent parameter on the requirements are shown in the following. We can classify f_1 and f_2 as the free independent variables and d_1 and d_2 as the dependent variables. However, we adopted the aforementioned classification.

5. Effects of Free Parameters

A qualified double-pass configuration needs to completely satisfy the aforementioned requirements, and several independent variables affect the fulfillment of the re-

quirements. Hence, it is necessary to set up an optical scheme with a set of constraints. In this section, we selected d_0 , d_1 , d_2 , and α as the independent free parameters. Some fixed parameters are given as $\alpha_{\max} = 5\%$, $R_{\text{col}} = 0.2$ m, $R_{\text{fiber}} = 1$ mm, $D_{f1} = 45$ mm, $D_{f2} = 100$ mm, $w_0 = 4.8$ mm, $M^2 = 7.8$, $s_1 = 1000$ mm, and $s_2 = 400$ mm. Here, these fixed parameters are chosen to be the same or similar to those in the present TST-2 Thomson scattering system [11]. For the temperature scale length, we set $a = 200$ mm, which is the typical minor radius of the TST-2 plasma [12].

In the following, we will show the effects of each parameter by scanning the parameter. The other parameters are fixed at those of a reference parameter set ($d_0 = 10$ m, $d_1 = 4$ m, $d_2 = 6$ m, and $\alpha = 5\%$), which is relatively close to the optimum, as shown in the following.

5.1 Effects of d_0 ($d_1 = 4$ m, $d_2 = 6$ m, $\alpha = 5\%$)

Figure 4(a) plots the normalized beam sizes on the first lens (blue), second lens (magenta), and fiber surface (red), calculated using Eqs. (2), (3), and (14) - (16), as well as the critical value of the requirement (horizontal dash line). It indicates that the normalized beam size requirements provide the lower and upper limits for the various d_0 . The normalized w_{f1} and w_{f2} increase as d_0 increases, whereas the normalized beam radius on the fiber surface ($4mw_p/D_{\text{fiber}}$) decreases because the longer d_0 would lessen the image size w_p .

The blue and red curves in Fig. 4(b) represent the normalized displacement of the backward beam on the first lens ($4w_{f1}/\delta_{f1}$) and the laser output ($4w_0/\delta_{\text{laser}}$), respectively. A red peak (at $d_0 \sim 5.5$ m) indicates the case where the backward beam would directly return to the laser output without any deviation of the backward beam from the originally forward path. This is the case where the red and yellow lines in Fig. 1 are intersecting at the laser output. Generally, with any given d_1 and d_2 , there is a small range of d_0 that jeopardizes the laser. The minimal displacement is located at the first lens when $d_0 < 8.5$ m, whereas it should be located near the laser output when $d_0 > 8.5$ m.

5.2 Effects of d_1 ($d_0 = 10$ m, $d_2 = 6$ m, $\alpha = 5\%$)

Figure 5 shows the results of the d_1 scan. Note that d_1 does not affect $4w_{f1}/D_{f1}$. As d_1 increases, the $4mw_p/D_{\text{fiber}}$ increases, whereas the $4w_{f2}/D_{f2}$ decreases (Fig. 5(a)). Moreover, the large focus size (w_p) induces a small divergence angle ($\theta = \lambda/\pi w_p$) of the Gaussian beam, so that the beam size on the second lens (w_{f2}) will be reduced with the increase of d_1 . As shown in Fig. 5(b), the increase of d_1 may deteriorate the relative collection efficiency (E_c) when the large d_1 leads to enough enlargement of the beam waist size in the plasma.

Figure 5(c) depicts the distribution of $4w_{f1}/\delta_1$ and

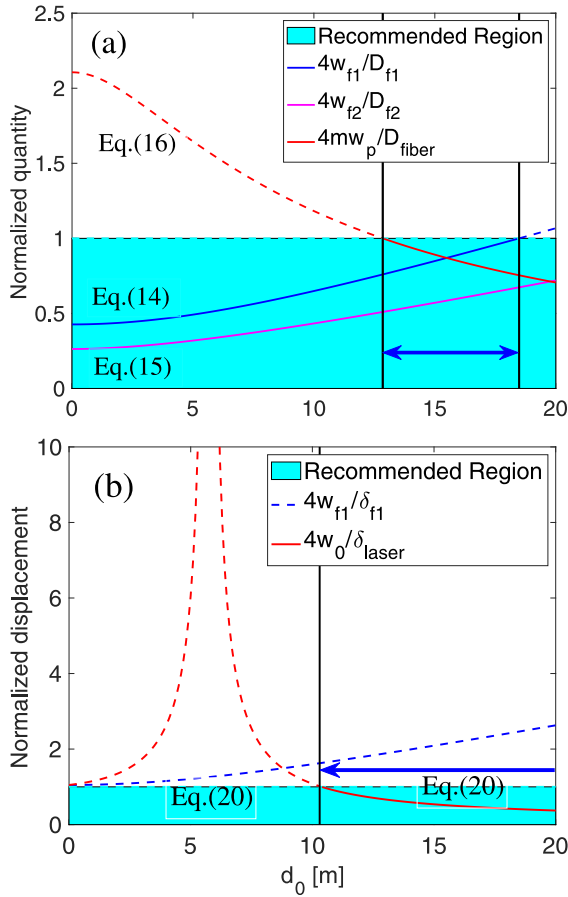


Fig. 4 The effects of d_0 on the (a) normalized beam size at the first lens, second lens, and fiber surface and (b) normalized displacement of the backward beam at the first lens and laser source. The recommended regions indicate the vertical regions satisfying the corresponding requirements. The numbers near the curves show the related equation number in Sec. 4. The horizontal thick arrows indicate the resultant d_0 region satisfying the corresponding requirements.

$4w_0/\delta_{laser}$ and a peak appears at $d_1 = 7.2$ m. The peak represents the case where the backward beam returns to the laser. The optimal position blocking the backward beam is located near the laser output when $d_1 < 4.8$ m, whereas it is located near the first lens when $d_1 > 4.8$ m.

5.3 Effects of d_2 ($d_0 = 10$ m, $d_1 = 4$ m, $\alpha = 5\%$)

In this case, d_2 affects the w_{f2} (Fig. 6 (a)), the normalized delay time $\Delta t_{pulse}/\Delta t_{delay}$ (Fig. 6 (b)), and the $4w_{f1}/\delta_{f1}$ and $4w_0/\delta_{laser}$ (Fig. 6 (c)). The normalized w_{f2} increases with d_2 , providing the performance of the configuration with an upper limit on d_2 . However, it is best to set a large d_2 to separate the backward scattering signal from the forward signal completely (as shown in the recommended region). Thus, the requirement of delay time introduces a lower limit into the available range of d_2 . As shown in Fig. 6 (c), the backward beam's displacement on

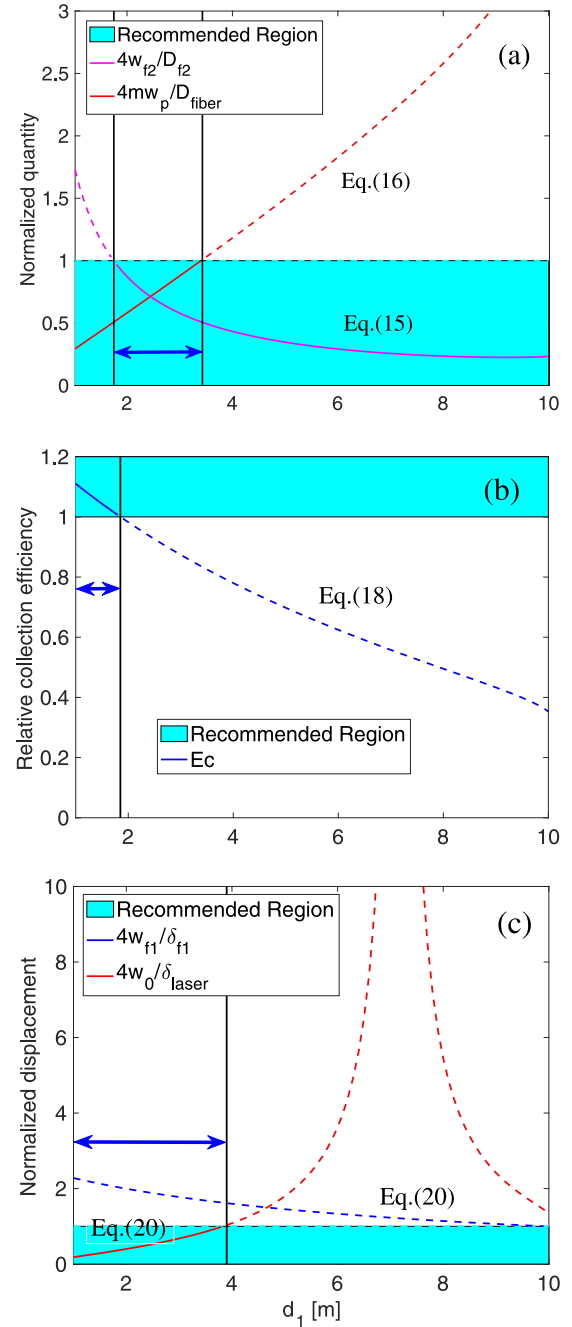


Fig. 5 The effects of d_1 on the (a) normalized beam size on the second lens and fiber surface, (b) relative collection efficiency of fiber, and (c) normalized displacement of the backward beam on the first lens and laser source. The recommended regions indicate the vertical regions satisfying the corresponding requirements. The numbers near the curves show the related equation number in Sec. 4. The horizontal thick arrows indicate the resultant d_1 region satisfying the corresponding requirements.

the first lens (δ_{f1}) drops inversely as d_2 increases ($\delta_{f1} = \delta_p(1 + d_1/d_2)$), and the normalized $4w_{f1}/\delta_{f1}$ will increase with a fixed δ_p . In contrast, the normalized $4w_0/\delta_{laser}$ will be reduced because of the backward beam's refraction passing through the first lens. Besides, there is no inter-

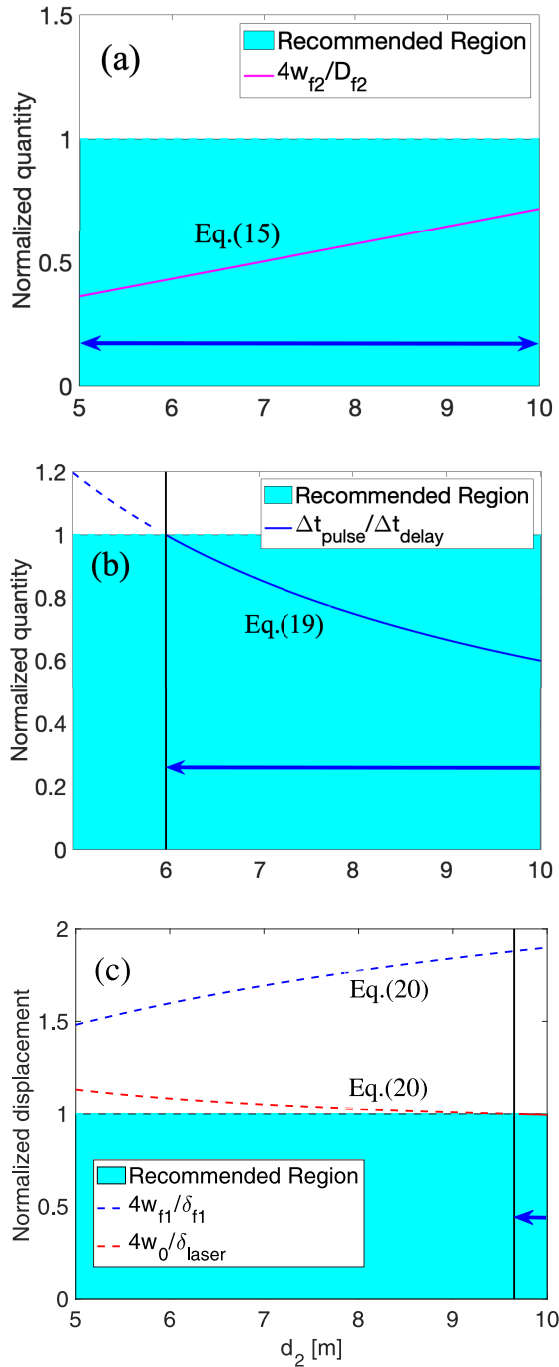


Fig. 6 The effects of d_2 on the (a) normalized beam size on the second lens, (b) normalized delay time between forward and backward scattering signals, and (c) normalized displacement of the backward beam on the first lens and laser source. The recommended regions indicate the vertical regions satisfying the corresponding requirements. The numbers near the curves show the related equation number in Sec. 4. The horizontal thick arrows indicate the resultant d_2 region satisfying the corresponding requirements.

section between $4w_{f1}/\delta_{f1}$ and $4w_0/\delta_{laser}$, and the optimal location preventing the backward beam is always near the laser output.

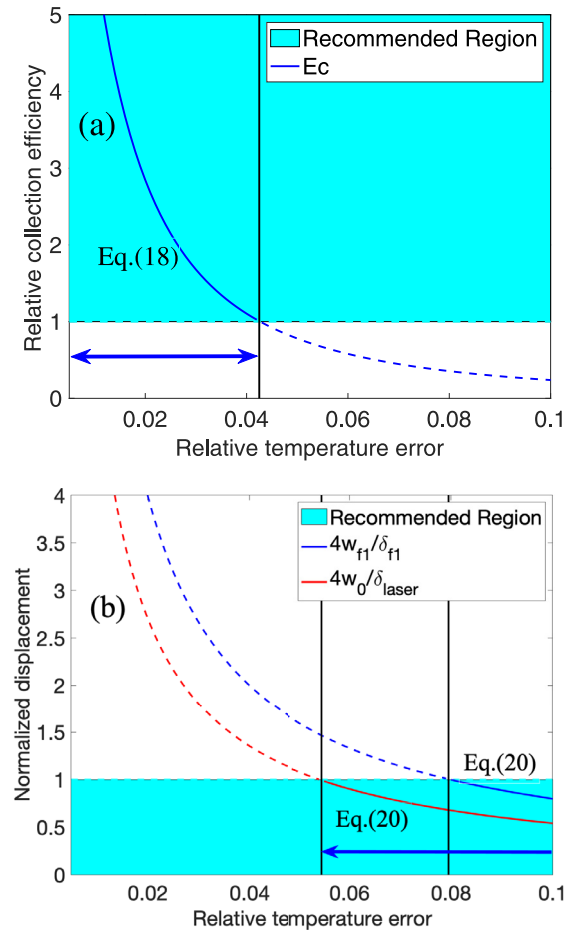


Fig. 7 The effects of relative temperature error (α) on the (a) relative collection efficiency and (b) normalized displacement of the backward beam on the first lens and laser source. The recommended regions indicate the vertical regions satisfying the corresponding requirements. The numbers near the curves show the related equation number in Sec. 4. The horizontal thick arrows indicate the resultant α region satisfying the corresponding requirements.

5.4 Effects of α ($d_0 = 10$ m, $d_1 = 4$ m, $d_2 = 6$ m)

A given relative temperature error (α) due to the spatial variation of the measured spot determines the backward beam's displacement at the scattering position (δ_p). With the increase of α , δ_p increases and the relative collection efficiency decreases (Fig. 7 (a)). The permissible maximum $\alpha_{max} = \Delta T_{max}/T$ is approximately 10%. Although 10% of the error is acceptable, the error due to α should be minimized because there are always other errors that arise due to different reasons. According to Fig. 7 (b), the two normalized displacements ($4w_{f1}/\delta_{f1}$ and $4w_0/\delta_{laser}$) decline simultaneously with the increase of α . Thus, the effects of α on the relative collection efficiency and the minimal normalized displacement of the backward beam qualitatively produce a lower and upper limit for the satisfaction of the requirement.

Although we have investigated the parametric dependences of all of the requirements in Sec. 5, it is useful to rank and extract the important and challenging requirements. The obtained rank would be useful for designing a double-pass configuration for the Thomson scattering measurements. For the double-pass configuration in Fig. 1, the requirements $4w_{f1}/D_{f1}$ and $4w_{f2}/D_{f2}$ would be relaxed when larger optical components could be used, while it is difficult to change the fibers' size (D_{fiber}) and the scattered signal's pulse width (Δt_{pulse}). Therefore, we will pay higher attention to several requirements to find out the optimal double-pass configuration in the following order: $\text{Min}\{4w_{f1}/\delta_{f1}, 4w_{\text{laser}}/\delta_{\text{laser}}\} > \Delta t_{\text{pulse}}/\Delta t_{\text{delay}} > 4mw_p/D_{\text{fiber}} > 4w_{f1}/D_{f1}$ and $4w_{f2}/D_{f2}$.

6. Optimization of the Double-Pass Configuration

This section presents the procedure for obtaining a few optimal configurations by fulfilling all the aforementioned requirements. Finding an optimum configuration is important because the optical parameters, such as the fabricated components' focal length, may not be accurate or chosen to the optimum value.

The double-pass configuration should ensure the measurement accuracy and reduce the backward beam's damage risk as much as possible. Hence, it is useful to regard $\text{Min}\{4w_{f1}/\delta_{f1}, 4w_{\text{laser}}/\delta_{\text{laser}}\}$ and $\alpha = \delta_p/a$ as the performance parameters. The former determines the damage risk, while the latter shows the possible systematic error of the measurements. Figure 8 gives an example of the optimization for $\delta\theta$ (which is equivalent to α). The increase of $\delta\theta$ strengthens the degree of safety, but the measurement quality would be degraded. Therefore, it is important to find the optimal configuration (i.e., free parameters' optimum set).

To optimize the configuration, we introduced the sum of the normalized requirement, which should be optimized as follows: $S \equiv 4w_{f1}/D_{f1} + 4mw_p/D_{\text{fiber}} + \Delta t_{\text{pulse}}/\Delta t_{\text{delay}} + 4w_{f2}/D_{f2} + \alpha/\alpha_{\text{max}} + \text{Min}\{4w_{f1}/\delta_{f1}, 4w_{\text{laser}}/\delta_{\text{laser}}\}$. It is very convenient to compare different cases because this is a single scalar. The smaller S case has more margin in the requirements, allowing fluctuations, instabilities, or fabrication errors in the parameters. The reason for excluding

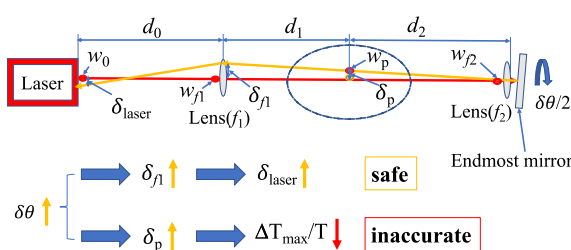


Fig. 8 Example of $\delta\theta$ optimization.

the three requirements, Eqs. (18), (21), and (22), from the criterion is their relative ease of attainment. Each normalized term in the S should be < 1 , and it is convenient to use S to find an optimum solution.

The solution in which all the requirements need to be satisfied and then S shows the minimum is searched by a program. For the simplest double-pass configuration (including two lenses and one mirror, as shown in Fig. 1), the corresponding optimal solution is $d_0 = 13.2$ m, $d_1 = 2.4$ m, $d_2 = 6.6$ m, $\alpha = 2.8\%$, $\delta\theta/2 = 0.029^\circ$, $D_{f1} = 45$ mm, $D_{f2} = 100$ mm, $f_1 = 2.14$ m, $f_2 = 6.61$ m, and its optimization S is 4.4. The beam radius along the optical pass is plotted in Fig. 9. The green horizontal dashed line represents the fiber's image radius in the plasma. It is a theoretical result, and some of them may be hard to achieve; for example, $d_0 = 13.2$ m is too long. It is desirable to shorten the d_0 by adding a few optical components (e.g., concave and convex lens). If an additional lens is placed somewhere between the laser output and the first lens (Fig. 10(a)), the optimization program produces the results of $l_1 = 3.4$ m, $ff_1 = -0.5$ m, $d_0 = 3.9$ m, $d_1 = 2.5$ m, $d_2 = 6$ m, $f_1 = 0.71$ m, $f_2 = 6.00$ m, $\alpha = 4\%$, $\delta\theta/2 = 0.042^\circ$, $D_{f1} = 45$ mm, $D_{f2} = 100$ mm, and its optimization criterion is 4.84. The corresponding beam radius behavior is displayed in Fig. 10(b). The results showed that it is possible to figure out an optimal configuration combined with its actual circumstance. The modified configuration also produces a symmetrical laser propagation against the endmost mirror.

In addition to the simple (Fig. 9) and modified configurations (Fig. 10), another simple configuration slightly breaks one of the requirements that is worthy of note. We relaxed a requirement as $\text{Min}\{4w_{f1}/\delta_{f1}, 4w_{\text{laser}}/\delta_{\text{laser}}\} \leq 1.1$, which does not break the requirement seriously because the factor of 4 makes enough margins left (Fig. 3). A set of parameters that establishes another simple configuration is $d_0 = 7.5$ m, $d_1 = 2.5$ m, $d_2 = 8.0$ m, $\alpha = 4\%$, $\delta\theta/2 = 0.032^\circ$, $D_{f1} = 45$ mm, $D_{f2} = 100$ mm, $f_1 = 2.24$ m, and $f_2 = 8.02$ m. Its corresponding beam radius behavior is shown in Fig. 11. Compared with the original simple con-

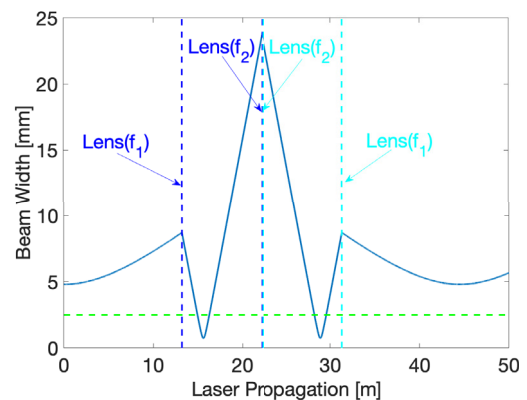


Fig. 9 Laser propagation without any additional lens.

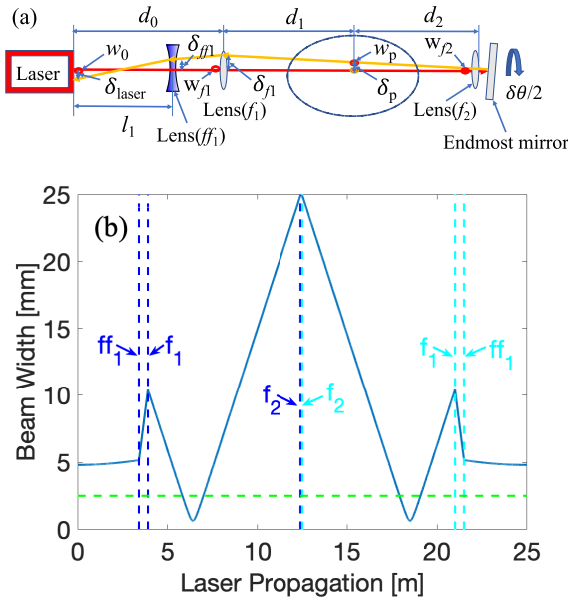


Fig. 10 (a) Modified configuration and (b) the corresponding laser propagation.

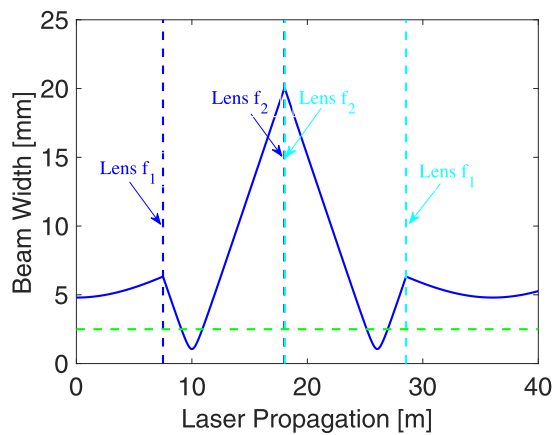


Fig. 11 Laser propagation of the second simple configuration.

figuration (Fig. 9), this second simple configuration shortens $d_0 = 13.2$ m to $d_0 = 7.5$ m, and it barely produces the requirement $\text{Min}\{4w_{f1}/\delta_1, 4w_{\text{laser}}/\delta_{\text{laser}}\} = 1.06$.

7. Conclusions

Double-pass Thomson scattering measurement is

a simple method to measure the electron temperature anisotropy in plasma. However, the damage risk to the laser device by the backward beam should be reduced. It could be achieved by placing the laser device away from the dangerous region (the vicinity of the intersection of the forward and backward beams). In this study, we proposed a double-pass configuration and a requirement list to reduce the risk while ensuring the measurement performance accuracy. Scanning the free parameters (d_0 , d_1 , d_2 , and α) reveals that the requirements have complicated relations with the free parameters and that it is difficult to conclude a simple expression to evaluate the double-pass configuration's performance. We proposed a numerical procedure to find the optimal configuration. We figured out two theoretically optimal solutions and one practically acceptable configuration through the optimization procedure based on the same or similar fixed parameters in the present TST-2 system. It is useful and applicable to the researchers who will design similar configurations because the optimal procedure is general. We selected the practically simple configuration shown in Fig. 11 ($d_0 = 7.5$ m, $d_1 = 2.5$ m, $d_2 = 8.0$ m, $\alpha = 4\%$, $\delta\theta/2 = 0.032^\circ$, $D_{f1} = 45$ mm, $D_{f2} = 100$ mm, $f_1 = 2.24$ m, and $f_2 = 8.02$ m) for TST-2 because of its shorter d_0 relative to the first simple configuration and its less optical components relative to the modified configuration.

Acknowledgments

This study is partly supported by the National Institute for Fusion Science Collaboration Research Program (NIFS18KOAR022 and NIFS12KUTR155).

- [1] M.D. Bowden *et al.*, J. Appl. Phys. **73**, 2732 (1993).
- [2] K. Muraoka *et al.*, Plasma Phys. Control. Fusion **40**, 1221 (1998).
- [3] J. Hiratsuka *et al.*, Plasma Fusion Res. **10**, 1402007 (2015).
- [4] J. Hiratsuka *et al.*, Plasma Fusion Res. **7**, 2402092 (2012).
- [5] A. Mase *et al.*, Rev. Sci. Instrum. **66**, 821 (1995).
- [6] J. Hiratsuka *et al.*, Plasma Fusion Res. **6**, 1202133 (2011).
- [7] H. Togashi *et al.*, Plasma Fusion Res. **9**, 1202005 (2014).
- [8] H. Togashi *et al.*, Rev. Sci. Instrum. **85**, 056103 (2014).
- [9] A. Ejiri *et al.*, Plasma Fusion Res. **5**, S2082 (2010).
- [10] S.A. Self, Appl. Opt. **22**, 658 (1983).
- [11] T. Yamaguchi *et al.*, Plasma Fusion Res. **5**, S2092 (2011).
- [12] Y. Takase *et al.*, Nucl. Fusion **41**, 1543 (2001).